Temperature and pressure manipulation of magnetic ordering and phonon dynamics with phase transition in multiferroic GdFeO₃: Evidence from Raman scattering

Yan Ye (叶艳),[1] Anyang Cui (崔安阳),[1] Mengyun Bian (卞梦云),[1] Kai Jiang (姜凯),[1] Liangqing Zhu (朱亮清),[1]
Jinzhong Zhang (张金中),[1] Liyan Shang (商丽燕),[1] Yawei Li (李亚巍) ●,[1] Zhigao Hu (胡志高),[1,2,3,*]
and Junhao Chu (褚君浩)[1,2,3]

[1]*Technical Center for Multifunctional Magneto-Optical Spectroscopy (Shanghai), Engineering Research Center of Nanophotonics &
Advanced Instrument (Ministry of Education), Department of Materials, School of Physics and Electronic Science,
East China Normal University, Shanghai 200241, China*
[2]*Collaborative Innovation Center of Extreme Optics, Shanxi University, Taiyuan, Shanxi 030006, China*
[3]*Shanghai Institute of Intelligent Electronics & Systems, Fudan University, Shanghai 200433, China*

We systematically investigate the detailed dynamics of the phonon and local structure of rare-earth ortho-ferrites GdFeO₃ single crystal with temperature and pressure induced structural/magnetic phase transition by Raman spectroscopy. Phonon evolution related to the motion of octahedra reveals paramagnetic to antiferromagnetic ordering transition of Fe^{3+} ions at Néel temperature $T_{N,Fe}$. By quantifying the polarized Raman spectra, especially the cross-polarized geometry, the lattice dynamics and distortion with local structure rearrangement during ferromagnetic transition has been also discovered. Particularly, we claim that the depolarization ratio could be quantified and used to precisely determine ferromagnetic phase transition of GdFeO₃ and symmetry evolution simultaneously. Additionally, pressure dependence (up to 25.03 GPa) of collective phonon behavior indicates that antiphase tilt in FeO₆ octahedra is more susceptible to the stress field than the in-phase one. The FeO₆ octahedra presents better compressible than GdO₁₂ dodecahedra in the GdFeO₃ lattice with respect to pressure. This work has discovered the physical mechanism underlying variation of local structural symmetry, octahedra tilt, and phonon dynamics in GdFeO₃, which can be regarded as the basic view for a series of GdFeO₃-type perovskites and more RFeO₃ system.

I. INTRODUCTION

Multiferroics attracts the broad scientific attention in material research, whose unusual physical properties simultaneously exhibit ferroelectric and magnetic ordering. Owing to the coupling characteristics of ferroelectricity and ferromagnetism, it is possible to apply external magnetic or electric field to control charge and spin in the bound system [1,2]. As a result, multiferroic matters would be regarded as potential candidate for creating multifunctional devices in unique designations, such as magneto-optical devices and spintronic devices [3–5]. As a typical class of multiferroic materials, rare-earth orthoferrites (RFeO₃) also witness renewed research interest due to their fascinating characteristics including magnetic modulation by temperature or electric field [6], spin reorientation [7], and magneto-optical effects [4].

RFeO₃ perovskites hold Pnma orthorhombic structure transferred from the distortions of ideal cubic phase with space group Pm$\bar{3}$m [8]. It also belongs to the canted antiferromagnetic (AFM) state resulting from the Dzyaloshinskii-Moriya interaction, presenting large antisymmetric exchange interactions in general [9]. Among the family members of

RFeO₃, GdFeO₃ (GdFO) is considered as the prototype of ABO₃ compounds with orthorhombic distortion. GdFeO₃ possesses three magnetic exchange interactions of Fe^{3+}-Fe^{3+}, Gd^{3+}-Gd^{3+}, and Fe^{3+}-Gd^{3+} [10]. These interactions contribute to different magnetic properties at various temperatures. Below the Néel temperature $T_{N,Fe} = 670$ K, paramagnetic ordering of GdFO turns to G-type AFM ordering along the a axis with weak ferromagnetic moment along the c axis due to the Fe^{3+}-Fe^{3+} interaction. A significant work from Tokunaga *et al.* has discovered the ferroelectric polarization below AFM ordering of Gd^{3+} ions, resulting from the striction by Fe^{3+}-Gd^{3+} exchange interaction in GdFO [11]. It allows the ferroelectric polarization and magnetization to be controlled by magnetic and electric field in GdFO compounds. Therefore, the physical characteristics of a multiferroic material are extremely sensitive to its lattice structure. Understanding structural properties in the typical class of GdFO crystal is of fundamental significance on many perovskites like RFeO₃, RMnO₃ and (Mg, Fe)SiO₃ [12].

Presently, the structure and phase transition of perovskites can be discovered by many tools. For instance, the structural evolution and phase transition of LaFeO₃ has been investigated by means of x-ray diffraction and powder neutron diffraction [13,14]. It has been reported on GdFeO₃ in the last decades that in order to study the Néel transition of Fe or Gd ions and focus on the spin-phonon coupling, it must be

024103-1

done via ^{57}Fe Mössbauer spectroscopy and Raman scattering [15,16]. On the other hand, pressure-dependent Raman spectra have been applied to reveal pressure dependence of mean Fe-O bond lengths in RFeO$_3$ [17]. Bhadram *et al.* considered that the Raman wave numbers of some modes would be sufficient to compare CrO$_6$ and RO$_{12}$ compressibility with pressure [18]. In other words, Raman spectroscopy has become a versatile technique to study molecule/lattice dynamics and distortions of perovskites solid solution [19–21]. It is not only considered to be an effective way to probe structural transitions in different condensed matter systems across the transition temperature [22,23], but also can be a powerful tool to investigate the spin-phonon and spin-lattice coupling [15,24]. The evolution of lattice structure could be obtained by analyzing the phonon behaviors and molecular vibrations with external factors like pressure, temperature, electric or magnetic field [17,23,25,26]. Therefore, it is reliable to investigate the structural behavior and phonon dynamics of GdFeO$_3$ comprehensively by temperature and pressure-dependent Raman spectroscopy. To the best of our knowledge, the polarized Raman scattering has not been used to explore the Néel temperature of GdFO by analyzing symmetry variation. In addition, all conclusions of pressure-dependent Raman spectroscopy mentioned above should be taken into consideration to provide a thorough view for GdFeO$_3$.

In this work, we systematically investigated and summarized the phonon and lattice dynamic of GdFeO$_3$ single crystal probed by temperature and pressure-dependent Raman spectra of both the unpolarized and polarized scattering geometries. The temperature dependence of depolarization ratio could give the Néel temperature exactly by following the change of structural symmetry. The Fe-O bond lengths related to in-phase and antiphase tilt mode shorten at different rate with pressure. The compressibility of FeO$_6$ and GdO$_{12}$ polyhedra was also analyzed. We provide a multiperspective and comprehensive physical study on magnetic phase transition, phonon, and lattice dynamics in the bound system of GdFO single crystal under various external fields. The present results could strengthen the understanding on the structure and multiferroic characteristics for more GdFO-based perovskite systems and structure evolution manipulated by temperature and pressure.

II. MATERIALS AND METHODS

The GdFeO$_3$ single crystal was synthesized by conventional solid-state reaction method [27]. The raw materials consist of Gd$_2$O$_3$ and Fe$_2$O$_3$ powders with 99.9% purity. At first, Gd$_2$O$_3$ was dried at 900 °C for 12 h to get rid of adsorbed water and CO$_2$. The mixture of Gd$_2$O$_3$ and Fe$_2$O$_3$ of ratio 1:1 was heated and grinded at 1150 °C for several days. Then, the sample was reground and pressed into two rods with 6-mm diameter under pressure. The rods were sintered at 1400 °C for 24 h in air. The crystal was grown by the feed and seed rods with a rotational speed of 25 rpm. Finally, the obtained single crystal was mechanically polished to erase the surface overlayer artifacts for Raman spectra measurements. Some parts of GdFO crystal were crushed into a powder for pressure-dependent experiments.
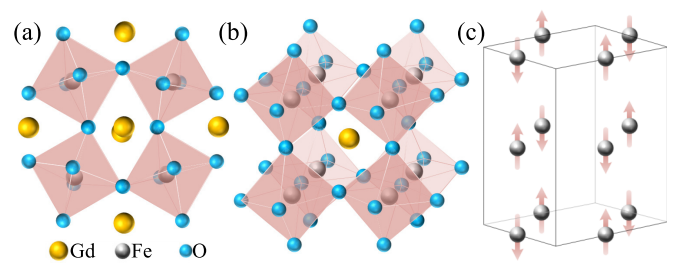

FIG. 1. (a) The front view and (b) 3D view of orthorhombic perovskite structure of GdFeO$_3$ with Pnma symmetry. (c) Schematics of Fe^{3+} spins structure for G-type antiferromagnetic ordering at Néel temperature.

Raman characterizations were carried out on a Jobin-Yvon LabRAM HR Evolution micro-Raman spectrometer with a spectral resolution of 1 cm^{-1}. Temperature dependent experiments from 80 to 700 K were performed by a Linkam THMSE 600 heating/cooling stage with a heating/cooling rate of 10 K/min and a temperature accuracy of ±0.1 K. A He-Ne laser with the wavelength of 632.8 nm was used as the excitation. The laser beam was focused through a 50× microscope with a working distance of 18 mm. All Raman spectra were eliminated with respect to the contribution of Bose-Einstein temperature factor. Polarized scattering measurements were performed with the aid of polarizers, which were placed in the excitation and detection path to define the paralleled-polarized (VV) and the crossed-polarized (VH) scattering geometries. Pressure-dependent Raman scattering measurements were recorded up to 25.03 GPa at room temperature. The powder of GdFO crystal was manually grinded and loaded into a tungsten gasket of 100 μm diameter in the diamond anvil cell (DAC) with diamond culets of 300 μm diameter. Silicone oil was used as the pressure-transmitting medium. Although the experimental data would be affected by the slow solidification of silicone oil, the sample in the DAC was in the state of hydrostatic pressure within the present range of stress field. The pressure was calibrated by the ruby luminescence method [28]. All spectra were reduced by $n(\omega, T)+1$ to eliminate the contribution of the Bose-Einstein temperature factor from the measured scattering intensity. The Bose-Einstein temperature factor is described as $n(\omega, T) = 1/[\exp(\hbar\omega/kT) - 1]$, where $\hbar$, ω, k, and T are the reduced Planck constant, phonon frequency, Boltzmann constant, and temperature, respectively. To quantify the phonon dynamics, Lorentzian-shaped deconvolution of the spectra were used according to the damped harmonic oscillator model.

III. RESULTS AND DISCUSSION

The single crystal GdFeO$_3$ crystallizes in the orthorhombic structure with centrosymmetric space group Pnma, as shown in Figs. 1(a) and 1(b). The GdFO lattice structure consists of the corner-sharing FeO$_6$ cation-centered octahedra with Gd^{3+} ions occupying the space of three-dimensional skeletons of octahedra. The octahedra tilt system cannot only be described as $a^-b^+a^-$ in Glazer's notation [29], but also be set as rotations by angles θ, φ, and ϕ around the $[101]_{pc}$, $[010]_{pc}$, and $[111]_{pc}$ axes, respectively [30]. The spin
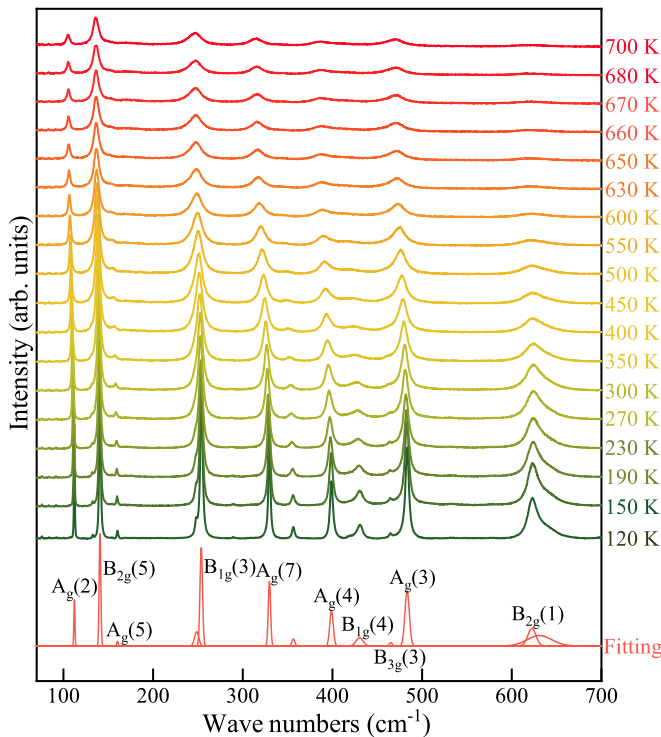
FIG. 2. Temperature dependence of unpolarized Raman spectra of $GdFeO_3$ and the corresponding Lorentzian fitting.
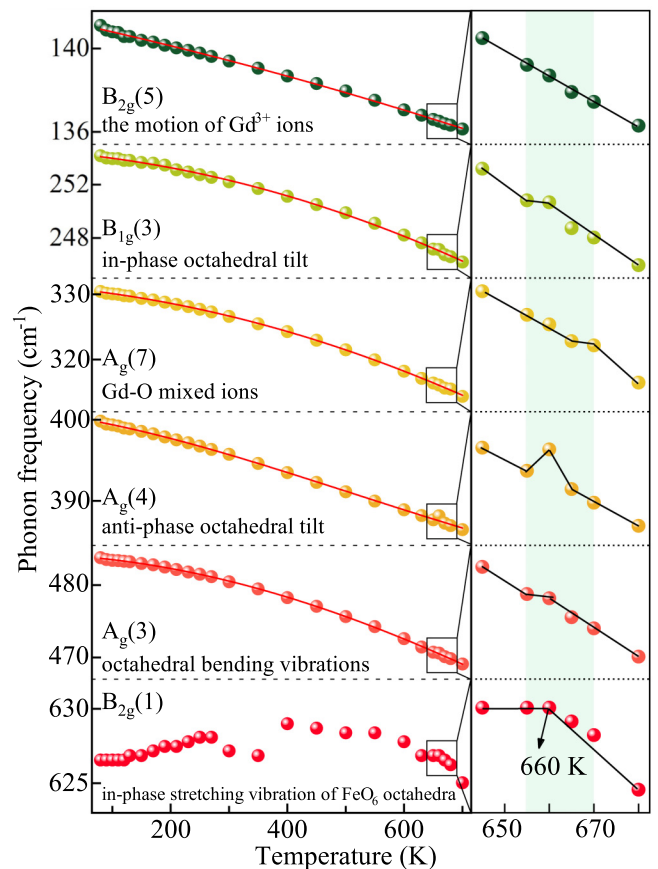

FIG. 3. The thermal evolution of phonon frequency for various vibrational modes and the red solid lines are the fitting curves based on the anharmonic model.

structure of the $G_x A_y F_z$ type in Bertaut's notation for the Fe sites is also presented in Fig. 1(c). G_x, A_y, and F_z is the spin components along the a, b, c axis of the orthorhombic unit cell with the NaCl-type, the layer-type antiferromagnetic and ferromagnetic-type configurations [31], respectively. The exchange striction, which is resulted from the eight nearest-neighbour Fe ions, would be offset in this G-type structure [32].

GdFeO$_3$ has several magnetic transitions like paramagnetic to weak ferromagnetic transition of Fe^{3+} ions (Néel transition ($T_{N,Fe}$)), spin-reorientation transition of Fe^{3+} ions ($T_{SRT,Fe}$) and AFM ordering of Gd^{3+} ions below 2.5 K, respectively. These magnetic transitions belong to second-order transition, exhibiting weak thermal hysteresis [33]. The Gd ions in GdFeO$_3$ are in the paramagnetic state within the temperature range of 80–700 K. In order to explore the evolution of phonons with the temperature, Raman spectral measurements are carried out, as shown in Fig. 2. According to group theory, GdFO has 24 Raman active modes, 28 infrared modes and 8 inactive modes given by the irreducible representation at the center of the Brillouin zone [24,34]: $\Gamma = 7A_g + 7B_{1g} + 5B_{2g} + 5B_{3g} + 8A_{1u} + 8B_{1u} + 10B_{2u} + 10B_{3u}$. The Lorentzian-shaped deconvolution of the spectra by the damped harmonic oscillator model is fitted and presented to specify the phonon frequency and its thermal evolution. As the temperature increases, almost all the modes are found to shift towards a lower frequency range, becoming broadly consistent with thermal expansion. Some modes of weak-intensity peak are even disappearing at higher temperatures. With increasing the temperature, however, the peaks are mostly broadening and merging with the

background signals. The number of phonons and phonon frequency have an intimate relationship to lattice symmetry and atomic distances.

The vibration modes associated with the displacement of rare earth ions are mainly located below 200 cm^{-1} involving $A_g(2)$, $B_{2g}(5)$ and $A_g(5)$, whereas phonon modes between 200 and 400 cm^{-1} are dominated by oxygen octahedral tilt modes including $B_{1g}(3)$, $B_{2g}(7)$, $A_g(7)$, and $A_g(4)$. The modes within 450–500 cm^{-1} are from the oxygen octahedral bending vibrations, while the mode at 625 cm^{-1} is related to in-phase stretching (breathing) vibration of FeO$_6$ octahedra. Figure 3 illustrates the evolution of phonon frequency as a function of temperature for some typical vibrational modes. It can be found that the magnitude of frequency shifts is different for various modes. While $B_{2g}(5)$ modes shows a shift about 5 cm^{-1}, the modes of $A_g(7)$ exhibits a larger shift of about 16 cm^{-1}. It indicated that the mode related to FeO$_6$ octahedra rotation are more sensitive to temperature than the mode dominated by Gd^{3+} ions. The evolution of the phonon frequency (ω) and full width at half maximum (Γ) with the temperature can be also described by the anharmonic model proposed by Balkanski [35]. The equation $\Gamma(T) = A[1 + \frac{2}{e^x - 1}] + B[1 + \frac{3}{e^y - 1} + \frac{3}{(e^y - 1)^2}]$ takes into account of fitting the frequency variation with temperature, where $x = \hbar\omega_0/2k_B T$, $y = \hbar\omega_0/3k_B T$, ω_0, A and B are adjustable parameters. Most
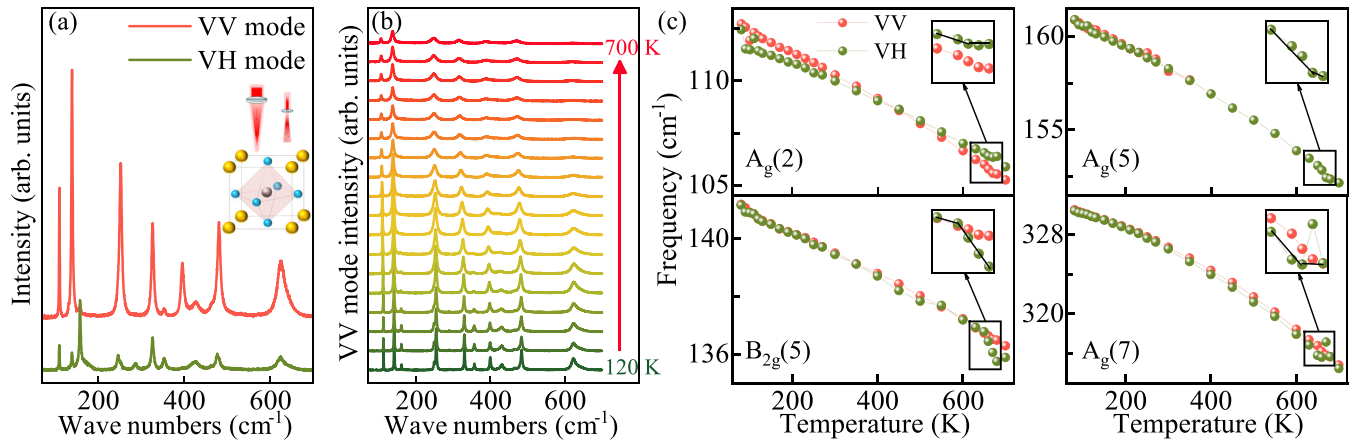
FIG. 4. (a) The VV-mode and VH-mode Raman spectra for $GdFeO_3$ at room temperature. (b) Temperature dependence of polarized Raman scattering in VV geometry. (c) The thermal evolution of phonon frequency in the VV and VH geometry for various phonon modes of $A_g(2)$, $B_{2g}(5)$, $A_g(5)$, and $A_g(7)$, respectively.

vibrational modes can be fitted well, as shown in Fig. 3, except for the mode of $B_{2g}(1)$. The frequency of the vibrational mode around 625 cm^{-1} moves first to higher frequency, and then to lower frequency as the temperature rises. It can be suggested that this anomalous phonon behavior may be attributed to a two-phonon mode or the impurities of crystal [36,37]. At the same time, the mode of $B_{1g}(3)$ at 254 cm^{-1} and $A_g(4)$ at 399 cm^{-1} present abnormal phenomena that the phonon frequency shifts to a higher range as temperature increases from 660 to 670 K. The $B_{1g}(3)$ and $A_g(4)$ modes represents the octahedra rotations around the $[010]_{pc}$ (in-phase) and the $[101]_{pc}$ (antiphase) axes. In the description of Landau theory, octahedra rotation is the order parameter for the phase transition from cubic phase with high symmetry [24]. Thus, the $B_{1g}(3)$ and $A_g(4)$ modes corresponding to $Q_{[010]_{pc}}$ and $Q_{[101]_{pc}}$, respectively, are the order parameters of Pnma structure for $GdFeO_3$-type perovskites. The anomalous phenomena of phonon frequency shift corresponding to the change of scattering peak are typically considered as one of the criteria to evaluate the change of crystal structure. It is well known that the phase transition of lattice structure is likely to bring abnormal changes in phonon frequency of vibrational modes. As we know, $RFeO_3$ compounds undergo a structural transformation of orthorhombic–rhombohedral–cubic at much higher temperatures, as compared to magnetic transition. Hence, we conclude that the temperature point of the abrupt change in phonon frequency is the Néel temperature of magnetic transition for Fe ions. Due to exchange striction, magnetic ions would displace, which further leads to the lattice expand or contract along the direction of interaction resulting in the coupling of phonon and spin [38,39]. In particular, the sudden change of the phonon behavior is resulted from the strong exchange striction around the magnetic transitions.

The polarized Raman scattering is regarded as a reliable technique to determine anisotropy and symmetry of lattice [40,41]. It also allows the phonon modes to assign vibrational symmetries and atomic displacements. As shown in Fig. 4(a), the scattering light is polarized by polaroids and collected by backscattering geometry. Raman spectra in the VV and VH geometries have been plotted in Fig. 4(a) for comparison. The peaks at 50–200 cm^{-1} related to motions of Gd^{3+} ions

are highly sensitive to the polarized orientation. The intensity of peak at 160 cm^{-1} corresponding to Gd^{3+} rotation under the VH geometry is much stronger than that under the VV configuration. The phonon mode of $A_g(4)$ is only active with VV scattering, while the $B_{2g}(7)$ mode is only active with VH scattering pattern. For comparison, the vibration modes related to FeO_6 otchaheral of $B_{2g}(1)$, $A_g(3)$, $A_g(7)$ are all active with different intensity in two kinds of polarized geometries. Temperature dependent Raman scattering including the VV and VH patterns have been performed from 80 to 700 K. Figure 4(b) shows temperature-dependent VV Raman scattering spectra, exhibiting similar behaviors with unpolarized ones as increasing the temperature. All peaks shift to higher frequency and become broadened with temperature. Some temperature dependences of phonon frequency in the VV and VH geometry are selected in Fig. 4(c). There are abnormal phenomena of frequency shift around 670 K solely recorded by the VH-mode Raman scattering, whereas it cannot be observed in the VV mode. It would be explained by the fact, which we observe that the $GdFeO_3$ crystal is anisotropic and/or has inhomogeneity in the local structural distortions.

Our previous study has clearly reported that the intensity of polarized Raman scattering could figure out the phonon characteristics and further reflecting lattice change [41]. The value of peak intensity could be given by

$$I \propto \frac{2\pi^3 \upsilon^4}{c^3}(\alpha_{F'F}\varepsilon_F)^2 = \frac{16\pi^4 \upsilon^4}{c^4}\alpha_{F'F}^2 I_0, \qquad (1)$$

where I, c, ω is the radiant energy, velocity of light in vacuum, and the phonon frequency, respectively, F represents x, y, or z axis, ε_F is defined as the electric field of incident light along the F axis, the incident energy is given by $I_0 \propto \frac{c}{8\pi}\varepsilon_F^2$ and $\alpha_{F'F}$ is the polarizability used to describe the polarization. The intensity of polarized Raman scattering is proportional to the polarizability, which becomes an important criterion to evaluate the symmetry and anisotropy of molecules. Figure 5(a) summarizes the thermal evolution of the normalized intensity of $A_g(2)$, $B_{2g}(5)$, $A_g(7)$, $B_{2g}(1)$ modes at the temperature range of 500–700 K. The polarized peak intensity gradually weakens within the temperature range, and only an obvious
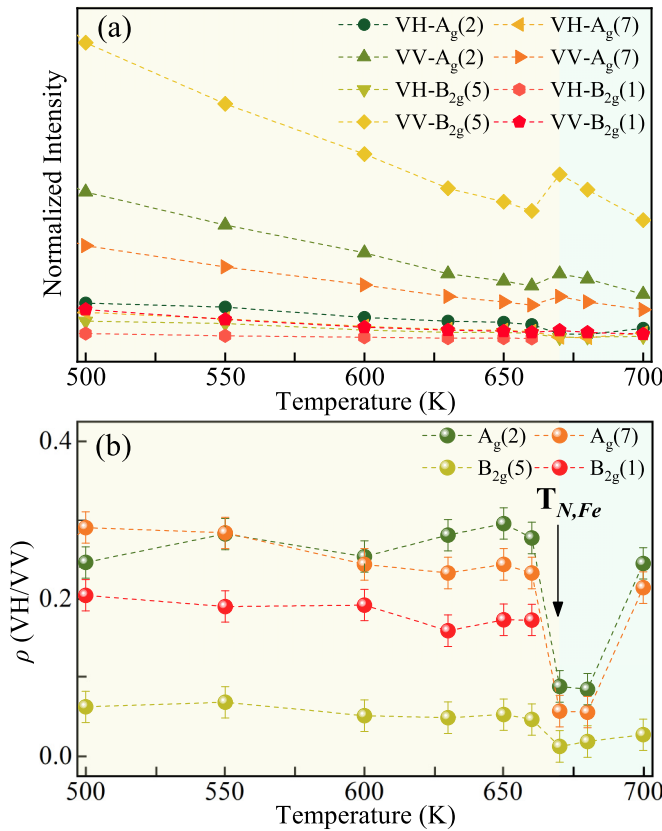
FIG. 5. Temperature dependence of (a) the normalized intensity and (b) depolarization ratio of polarized scattering for $A_g(2)$, $B_{2g}(5)$, $A_g(7)$, and $B_{2g}(1)$ modes, respectively.

FIG. 6. Pressure dependence of Raman spectra observed at room temperature within the pressure range of 0.11–25.03 GPa.

anomaly in frequency shift occurs around 670 K. It indicates that GdFeO₃ has a magnetic phase transition at 670 K.

Apart from two basic parameters of the phonon frequency and intensity of Raman scattering, the depolarization ratio (ρ_l) is the third important parameter to distinguish the thermal-induced lattice structural evolution and phase transition of GdFO. The value of ρ_l is given by

$$\rho_l = \frac{I_{VH}}{I_{VV}} = \frac{3\beta^2}{45\bar{\alpha} + 4\beta^2}, \qquad (2)$$

where $\bar{\alpha}$ is the average of polarizability along three primary crystallographic axes, and β^2 presents the degree of anisotropy [42,43]. The depolarization ratio, regarded as a key parameter, represents the degree of anisotropy with its difference and indicates the symmetry evolution. Figure 5(b) plots the temperature-dependent depolarization ratio $\rho_l(T)$ of vibrational modes of $A_g(2)$, $B_{2g}(5)$, $A_g(7)$, and $B_{2g}(1)$. The value of depolarization ratio for $A_g(2)$ and $A_g(7)$ modes becomes stable with the temperature, where only a sudden drop occurs at 670–680 K. Local structure rearrangement of GdFO, which may result from the exchange striction, was discovered across $T_{N,Fe}$ [14,15]. This is the signature of a second order magnetic phase transition, where exchange striction would induce concomitant changes in bond lengths and atomic positions. A tiny local distortion in the positions of atoms has already resulted in the sudden change of symmetry. In other words, the crystalline structure can change
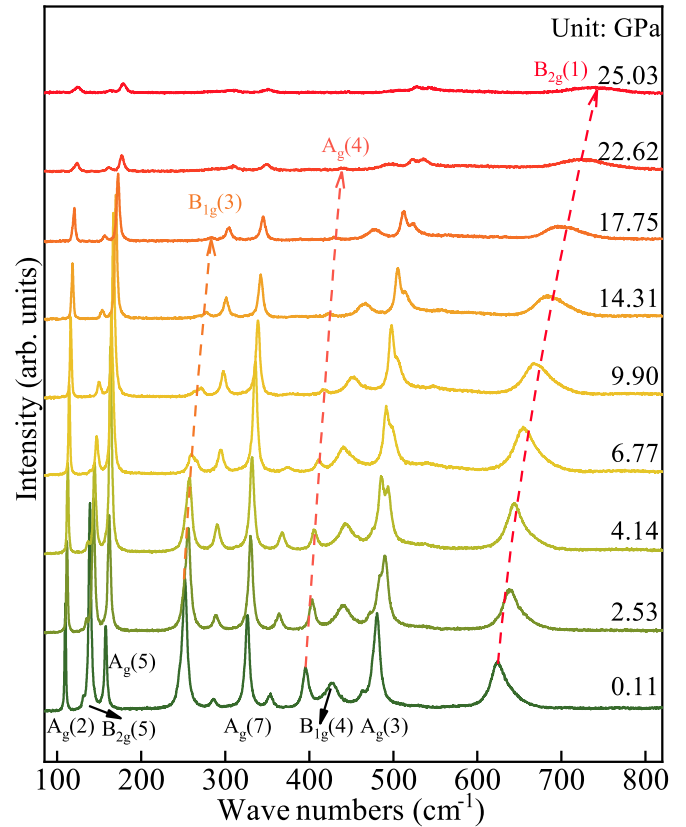
continuously or discontinuously, but the symmetry change can only be abrupt. Hence, it reasonably corresponds to the abrupt changes during the process of the magnetic phase transition, which is generally expected to be second order. As for the $B_{2g}(1)$ mode, the depolarization ratio has no value when the temperature is higher than 670 K. The molecular geometry could be judged by the value of depolarization ratio. If $\rho_l(T)$ (less than 0.75) approaches to 0, it illustrates a better symmetry of vibration configuration. The $\rho_l(T)$ value of $B_{2g}(5)$ mode is generally lower than that of $A_g(2)$ mode, representing the higher symmetric geometry of molecular vibrational configuration. The ratio is close to zero resulting from the spherical symmetry due to the anisotropic degree $\beta^2 = 0$. The behavior of polarized Raman scattering is more obvious than that of the unpolarized one. Therefore, the analysis of temperature dependent polarized intensity and depolarization ratio reveals the thermal-induced lattice symmetry of GdFO during the magnetic transition.

Recently, hydrostatic pressure has been gradually taken into considerations to study critical phenomena. It would permit the change of the interatomic distances so that pressure gives rise to the interactions to a greater extent than other external factor like temperature. As for the phonon and lattice behavior of GdFeO₃ under stress field, we also carried out pressure-dependent Raman scattering measurements at room temperature up to 25.03 GPa. Figure 6 presents the evolution of Raman spectra with pressure to probe the lattice distortions. The unit cell is compressed resulting from increasing the
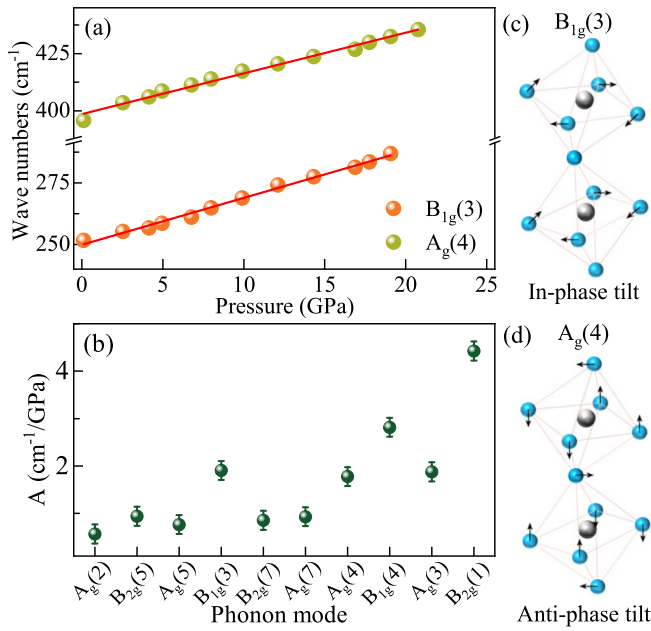
FIG. 7. (a) Pressure dependence of phonon frequency and intensity of $B_{1g}(3)$ and $A_g(4)$ mode. The red solid lines are linear fittings. (b) The pressure coefficients for each vibrational mode. (c) and (d) Schematic representations of vibrations of in-phase tilt and antiphase tilt.

pressure. This situation would lead to the variation of the FeO_6 octahedral tilt at respective pressure, which contributes to significant changes in the Raman spectra. Therefore, all the phonon modes shift to the higher frequencies and become broader owing to shorter bond and volume reduction due to increasing the pressure. The intensity of phonon modes weakens and some peaks disappear eventually burying in the background signals as presented in Fig. 6. Note that it has been reported that the RFeO$_3$ compounds has a first-order isostructural insulator-to-metal phase transition beyond 40 GPa [17]. In the available pressure range, GdFeO$_3$ lattice does not present structural transformation.

The frequency of phonon modes [$B_{1g}(3)$ and $A_g(4)$] were plotted as a function of pressure to exhibit more details of frequency shift with pressure in Fig. 7(a). As previously mentioned, the $B_{1g}(3)$ and $A_g(4)$ modes corresponding to in-phase and antiphase tilt are assigned to the FeO_6 octahedral rotations, which are major order parameters related to the lowering symmetry [8]. The phonon frequency of these modes shifts to higher frequency about 30 cm^{-1}. Compared to temperature dependence of frequency, pressure has the greater effect on phonon variations. As shown in Fig. 7(a), the in-phase [$B_{1g}(3)$] and antiphase [$A_g(4)$] tilt behaviors disappear when the pressure reaches over 20 GPa. It indicates that the local symmetry presents some variations owing to the structural adjustment to accommodate the external pressure. Figures 7(c) and 7(d) exhibit the three-dimensional view of two vibrational modes. In orthorhombic perovskites, the in-phase and antiphase tilts along the $[010]_{pc}$ and $[101]_{pc}$ directions of pseudo-cubic would transform on the basis of the M_3^+ and R_4^+ irreducible representations of the $Pm\bar{3}m$ space group, respectively [29,44]. Raman scattering was utilized to explore

the pressure-induced tilt angles and octahedra distortions. The frequency (ω) of in-phase and antiphase tilt modes follows a linear correlation with the mean length of Fe-O bond ($\langle Fe\text{-}O \rangle$) and FeO_6 tilt angle (θ) [17,45], which could be given as follows:

$$\omega = (a\langle Fe - O \rangle + b)\theta, \qquad (3)$$

where the fitting parameters $a = -42.3$ cm^{-1}/Å deg and $b = 109.1$ cm^{-1}/deg, respectively [44]. Furthermore, the relationship between the pressure and wave number of the tilt mode is expressed by

$$\frac{d\omega}{dP} = [a + b\langle Fe - O \rangle(P)]\frac{d\theta}{dP} + a\theta(P)\left(\frac{d\langle Fe - O \rangle}{dP}\right). \quad (4)$$

As $\frac{d\omega}{dP}$ is the slope of the function of pressure-dependent wave numbers and other parameters were referred [44,45], we obtained $\frac{d\langle Fe-O \rangle}{dP} = -0.0046 \pm 0.0001$, -0.0026 ± 0.0002 Å/deg for in-phase and antiphase tilt, respectively. The bond lengths for both tilt modes reduce under pressure. These obtained values of $\frac{d\langle Fe-O \rangle}{dP}$ illustrate that the mean bond length of in-phase tilt decreases at a larger rate than that of antiphase tilt as the pressure increases. The bond lengths could reflect the degree of octahedral distortion, which demonstrates the mechanism of pressure accommodation.

On the other hand, the relative compressibility of the BO_6 octahedra and AO_{12} dodecahedra plays an important role in understanding the structural stability with pressure increasing. In order to find out the structural evolution of GdFeO$_3$, we focus on the slope of pressure dependent frequency of every observed mode. According to a regular rule about the pressure dependence of phase sequence based on bond-valence concept [12], the ratio of compressibility (M_A/M_B) of AO_{12} and BO_6 less or more than unity would allow us to determine the perovskite to become more distorted or less with the external pressure increasing. In terms of GdFeO$_3$, the case of $M_A/M_B > 1$ points out that the FeO_6 octahedra are more compressible than GdO_{12} dodecahedra and GdFO would transfer to higher symmetry phase with increasing the pressure [46]. However, many of 3:3 perovskites do not follow this regular rule. For example, previous reports pointed out that RFeO$_3$ and RCrO$_3$ with smaller R ions turn to more distorted structures with the pressure [17,18]. Here, all the measured frequency of each phonon could be fitted according to a linear-related function with respect to pressure, following $\Delta\omega(P) = A \times P$, where parameter A is first-order pressure coefficient. The value of each pressure coefficient for phonon mode was given in Fig. 7(b). Particularly, $B_{2g}(1)$ mode, representing the antistretching vibration of FeO_6 octahedra, has the largest value of pressure coefficient. It may be attributed to high sensitivity to the changes in Fe-O bond lengths inside octahedra for the frequency of the $B_{2g}(1)$ mode. The in-phase and antiphase tilt modes [$B_{1g}(3)$ and $A_g(4)$] have a similar value of pressure coefficient. On the contrary, the value of pressure coefficient for GdO_{12} sites corresponding to the $A_g(7)$ mode is smaller than the ones for most modes related to octahedra like $B_{1g}(3)$, $A_g(3)$ and $B_{2g}(1)$. The compressions at A and B sites are anisotropic owing to the presence of bonds with different length in orthorhombic ABO_3 [47]. Hence, the

frequencies of $B_{2g}(1)$ and $A_g(7)$ modes, which rely on the average Fe-O and Gd-O bond lengths, would be sufficient to compare the related FeO_6 and GdO_{12} compressibility with pressure qualitatively. As a result, these values also indicate that the GdO_{12} dodecahedra are less compressible than FeO_6 sites with pressure.

The radius of R^{3+} ions can adjust the octahedral distortion continuously in orthorhombic perovskites. It has been reported that the octahedral distortion of these orthoferrites with larger size of R^{3+} suppressed with increasing the pressure experimentally and theoretically, while the rare-earth cations smaller than Gd^{3+} have the opposite pressure-dependent behaviors [17,48]. We believe that the rule of relative polyhedral compressibility is suitable for $GdFeO_3$ and these orthoferrites with rare-earth ions larger than Gd^{3+}, but may not be suitable for orthoferrites with rare-earth ions smaller than Gd^{3+}.

IV. CONCLUSION AND OUTLOOK

This work systematically demonstrates the temperature and pressure dependence of ferromagnetic ordering, lattice and phonon behaviors on $GdFeO_3$ single crystal through unpolarized and polarized Raman spectroscopy. The Néel temperature of Fe^{3+} ions has been observed around 670 K under the thermal field. Particularly, it is proven that the polarized scattering performs higher sensitivity than the unpolarized one to detect the local symmetry and anisotropy of lattice induced by magnetic transition. Thus, we reveal that the magnetic ordering transition at 670 K is accompanied with the local structure and symmetry change by quantifying temperature dependent depolarization ratio. The concept of depolarization ratio could be applied into studying magnetic transition of $RFeO_3$ compounds.

Moreover, pressure dependence of phonon evolution indicates that the octahedral tilt behavior plays the key role in local structure of $GdFeO_3$ lattice. Especially, we indicate that the mean bond length of in-phase tilt decreases at a larger rate than that of antiphase tilt with pressure. The external pressure makes a greater effect on the compressibility of FeO_6 octahedra than that of GdO_{12} dodecahedra, which is supported by comparing the frequencies shift of $B_{2g}(1)$ and $A_g(7)$ modes. This work provides a solid and thorough investigation on probing the ferromagnetic ordering, lattice, and phonon dynamics of $GdFeO_3$-type perovskites. And the present methods and results based on Raman scattering technique are of fundamental importance for dissecting the structure property and ferromagnetism tuned by various physical fields on $GdFeO_3$-type perovskites and more $RFeO_3$ solid solutions.

[1] R. Ramesh and N. A. Spaldin, Nat. Mater. **6**, 21 (2007).

[2] S.-W. Cheong and M. Mostovoy, Nat. Mater. **6**, 13 (2007).

[3] D. Bossini, D. Malik, B. Redlich, A. F. G. van der Meer, R. V. Pisarev, T. Rasing, and A. V. Kimel, Phys. Rev. B **87**, 085101 (2013).

[4] J. A. de Jong, A. V. Kimel, R. V. Pisarev, A. Kirilyuk, and T. Rasing, Phys. Rev. B **84**, 104421 (2011).

[5] Y. K. Jeong, J. H. Lee, S. J. Ahn, and H. M. Jang, Solid State Commun. **152**, 1112 (2012).

[6] Y. Tokunaga, Y. Taguchi, T. Arima, and Y. Tokura, Nat. Phys. **8**, 838 (2012).

[7] W. Slawinski, R. Przeniosko, I. Sosnowska, and E. Suard, J. Phys.: Condens. Matter. **17**, 4605 (2005).

[8] J. M. Perez-Mato, D. Orobengoa, and M. I. Aroyo, Acta Crystallogr. Sect. A **66**, 558 (2010).

[9] J. D. Cashion, A. H. Cooke, D. M. Matin, and M. R. Wells, J. Phys. C **3**, 1612 (1970).

[10] R. L. White, J. Appl. Phys. **40**, 1061 (1969).

[11] Y. Tokunaga, N. Furukawa, H. Sakai, Y. Taguchi, T. Arima, and Y. Tokura, Nat. Mater. **8**, 558 (2009).

[12] J. Zhao, N. L. Ross, and R. J. Angel, Acta Crystallogr. Sect. B **60**, 263 (2004).

[13] C. A. L. Dixon, C. M. Kavanagh, K. S. Knight, W. Kockelmann, F. D. Morrison, and P. Lightfoot, J. Solid State Chem. **230**, 337 (2015).

[14] S. M. Selbach, J. R. Tolchard, A. Fossdal, and T. Grande, J. Solid State Chem. **196**, 249 (2012).

[15] A. Panchwanee, V. R. Reddy, A. Gupta, and V. G. Sathe, Mater. Chem. Phys. **196**, 205 (2017).

[16] A. Panchwanee, S. K. Upadhyay, N. P. Lalla, V. G. Sathe, A. Gupta, and V. R. Reddy, Phys. Rev. B **99**, 064433 (2019).

[17] R. Vilarinho, P. Bouvier, M. Guennou, I. Peral, M. C. Weber, P. Tavares, M. Mihalik, Jr., M. Mihalik, G. Garbarino, M. Mezouar, J. Kreisel, A. Almeida, and J. A. Moreira, Phys. Rev. B **99**, 064109 (2019).

[18] V. S. Bhadram, D. Swain, R. Dhanya, M. Polentarutti, A. Sundaresan, and C. Narayana, Mater. Res. Express **1**, 026111 (2014).

[19] J. Laverdière, S. Jandl, A. A. Mukhin, V. Y. Ivanov, V. G. Ivanov, and M. N. Iliev, Phys. Rev. B **73**, 214301 (2006).

[20] D. A. Mota, A. Almeida, V. H. Rodrigues, M. M. R. Costa, P. Tavares, P. Bouvier, M. Guennou, J. Kreisel, and J. A. Moreira, Phys. Rev. B **90**, 054104 (2014).

[21] R. Vilarinho, E. C. Queirós, A. Almeida, P. B. Tavares, M. Guennou, J. Kreisel, and J. A. Moreira, J. Solid State Chem. **228**, 76 (2015).

[22] A. Y. Cui, K. Jiang, P. Zhang, L. P. Xu, G. S. Xu, X. M. Chen, Z. G. Hu, and J. H. Chu, J. Phys. Chem. C **121**, 14322 (2017).

[23] J. Z. Zhang, W.-Y. Tong, J. J. Zhu, J. Y. Xu, Z. H. Duan, L. P. Xu, Z. G. Hu, C.-G. Duan, X. J. Meng, Z. Q. Zhu, and J. H. Chu, Phys. Rev. B **91**, 085201 (2015).

[24] M. C. Weber, M. Guennou, H. J. Zhao, J. Iniguez, R. Vilarinho, A. Almeida, J. A. Moreira, and J. Kreisel, Phys. Rev. B **94**, 214103 (2016).

[25] M. Chen, Y. Wang, C. Huang, W. Wang, and H. Chui, J. Phys. D **51**, 385303 (2018).

[26] M. Kim, X. M. Chen, Y. I. Joe, E. Fradkin, P. Abbamonte, and S. L. Cooper, Phys. Rev. Lett. **104**, 136402 (2010).

[27] Y. Zhou, Y. X. Ye, J. F. Wang, Z. W. Jiao, J. J. Zhang, and T. Gao, Ferroelectrics **488**, 18 (2015).

[28] H. K. Mao, J. Xu, and P. M. Bell, J. Geophys. Res. **91**, 4673 (1986).

[29] A. M. Glazer, Acta Crystallogr. Sect. B **28**, 3384 (1972).

[30] R. H. Mitchell, *Perovskites: Modern and Ancient* (Almaz Press, Ontario, 2002).

[31] E. F. Bertaut, *Magnetism* (Academic, New York, 1963), Vol. 3.

[32] D. C. Cook and J. D. Cashion, J. Phys. C **13**, 4199 (1980).

[33] S. Yang, X. B. Ren, and X. P. Song, Phys. Rev. B **78**, 174427 (2008).

[34] E. Kroumova, M. Aroyo, J. Perez-Mato, A. Kirov, C. Capillas, S. Ivantchev, and H. Wondratschek, Phase Trans. **76**, 155 (2003).

[35] M. Balkanski, R. F. Wallis, and E. Haro, Phys. Rev. B **28**, 1928 (1983).

[36] N. Koshizuka and S. Ushioda, Phys. Rev. B **22**, 5394 (1980).

[37] S. Venugopalan, M. Dutta, A. K. Ramdas, and J. P. Remeika, Phys. Rev. B **31**, 1490 (1985).

[38] S. Greenwald and J. S. Smart, Nature (London) **166**, 523 (1950).

[39] J. S. Smart and S. Greenwald, Phys. Rev. **82**, 113 (1951).

[40] S. Klauer and M. Wöhlecke, Phys. Rev. Lett. **68**, 3212 (1992).

[41] A. Y. Cui, Y. Ye, L. M. Zheng, K. Jiang, L. Q. Zhu, L. Y. Shang, Y. W. Li, Z. G. Hu, and J. H. Chu, Phys. Rev. B **100**, 024102 (2019).

[42] D. A. Long, *Raman Spectroscopy* (McGraw-Hill, New York, 1977).

[43] C. Banwell and E. McCash, *Fundamentals of Molecular Spectroscopy* (McGraw-Hill, New York, 1994).

[44] M. A. Carpenter and C. J. Howard, Acta Crystallogr. Sect. B **65**, 134 (2009).

[45] N. D. Todorov, M. V Abrashev, and V. G. Ivanov, J. Phys.: Condens. Matter. **24**, 175404 (2012).

[46] R. J. Angel, J. Zhao, and N. L. Ross, Phys. Rev. Lett. **95**, 025503 (2005).

[47] N. L. Ross, J. Zhao, and R. J. Angel, J. Solid State Chem. **177**, 3768 (2004).

[48] H. J. Xiang, M. Guennou, J. Íñiguez, J. Kreisel, and L. Bellaiche, Phys. Rev. B **96**, 054102 (2017).